AIP | Review of Scientific Instruments

Cryogenic probe station for on-wafer characterization of electrical devices

Damon Russell, Kieran Cleary, and Rodrigo Reeves

Citation: Rev. Sci. Instrum. **83**, 044703 (2012); doi: 10.1063/1.3700213
View online: http://dx.doi.org/10.1063/1.3700213
View Table of Contents: http://rsi.aip.org/resource/1/RSINAK/v83/i4
Published by the American Institute of Physics.

Cryogenic probe station for on-wafer characterization of electrical devices

Damon Russell,[a] Kieran Cleary,[b] and Rodrigo Reeves[c]
California Institute of Technology, Pasadena, California 91107, USA

(Received 27 January 2012; accepted 17 March 2012; published online 9 April 2012)

A probe station, suitable for the electrical characterization of integrated circuits at cryogenic temperatures is presented. The unique design incorporates all moving components inside the cryostat at room temperature, greatly simplifying the design and allowing automated step and repeat testing. The system can characterize wafers up to 100 mm in diameter, at temperatures <20 K. It is capable of highly repeatable measurements at millimeter-wave frequencies, even though it utilizes a Gifford McMahon cryocooler which typically imposes limits due to vibration. Its capabilities are illustrated by noise temperature and S-parameter measurements on low noise amplifiers for radio astronomy, operating at 75–116 GHz. © *2012 American Institute of Physics*. [http://dx.doi.org/10.1063/1.3700213]

I. INTRODUCTION

Indium phosphide (InP) high electron mobility transistors (HEMTs) remain the lowest noise temperature devices for use in cryogenic microwave and millimeter wave receiver front ends through W-band (75–110 GHz), where noise temperatures <30 K have been reported.[1,2] Future instruments for radio-astronomy will utilize large numbers of these devices, operating at frequencies up to 116 GHz, to meet the sensitivity and survey speed requirements of future experiments. These devices may be individual discrete transistors or integrated as part of a monolithic microwave integrated circuit (MMIC).

Unfortunately, InP has not seen the same developmental pace as technologies such as silicon, and as a result the yield of low noise InP devices, especially at cryogenic temperatures, is usually <50%. Traditionally, it has been necessary to package a device in order to evaluate its performance cryogenically. This is especially true of devices operating at W-band, due to the difficulties imposed by wafer probing at these frequencies. The investment associated with the packaging and testing of each device dramatically increases the cost and therefore imposes practical limits on the number of devices screened for a given instrument. In addition, it is desired to reduce the noise of current state of the art devices, which is currently about 5 times the quantum limit (hf/k), to improve the capabilities of existing instruments.

To speed the evaluation of existing devices, as well as improve the development cycle time of new ones, the need exists for a cryogenic probe station for the measurement of wafers at frequencies up to 116 GHz, allowing devices to be rapidly tested without the investment in packaging. Although several excellent commercial systems exist for cryogenic probing, their designs impose certain limitations for use in measurements at millimeter wave (30–300 GHz) frequencies, as will be discussed further. Furthermore, most of these stations employ liquid helium (LHE) for cooling, yielding higher operating costs than the station presented here which uses a closed-cycle cryocooler.

Section II of this paper details the design of the cryogenic probe station, shown in Figure 1. Its capabilities are summarized in Table I and are demonstrated in Sec. III, where noise temperature and S-parameter measurements are presented for a W-band low noise amplifier (LNA). Sec. IV discusses further improvements to the station.

II. DESIGN

Commercial cryogenic probe stations commonly employ one of two methods to move their probes relative to the chuck. The first approach is to keep the chuck position fixed and move the entire platen (probes remaining in the same relative position to the platen) across the wafer. This is a particularly attractive approach for probe stations cooled by LHE in an open flow configuration, as the chuck may be mounted directly to the cold head, minimizing its temperature. The primary drawback of such a configuration is that all cabling to the probes must translate the range of motion of the platen. Although feasible at lower microwave frequencies, where coaxial cable can be used, this becomes intractable at millimeter wave frequencies where waveguide must be used due to loss considerations. Another common approach is fix the chuck and move the probe positioners, located external to the cryostat through bellows and long probe arms. Although this eases some cabling issues, it creates two problems: each probe must be moved in the testing of multiple devices, making step and repeat testing over large areas time intensive; and potential loss of calibration when the probes are moved a significant distance from their initial calibration positions. The use of long probe arms also introduces stability concerns, due to their lower natural resonance frequency.

To overcome these problems, the probe station presented here uses precision translation stages to move the chuck over its required range. The chuck is pistoned up (measurement) and down (movement) via a stepper motor actuated mechanism, located below the chuck, allowing for step and repeat measurement capability. The probe positioners located on the platen are used only to position the probes in their relative configuration, and only small movements are required after the initial setup has been completed. The system is unique,

[a]Electronic mail: drussell@caltech.edu.
[b]Electronic mail: kcleary@astro.caltech.edu.
[c]Electronic mail: rreeves@astro.caltech.edu.

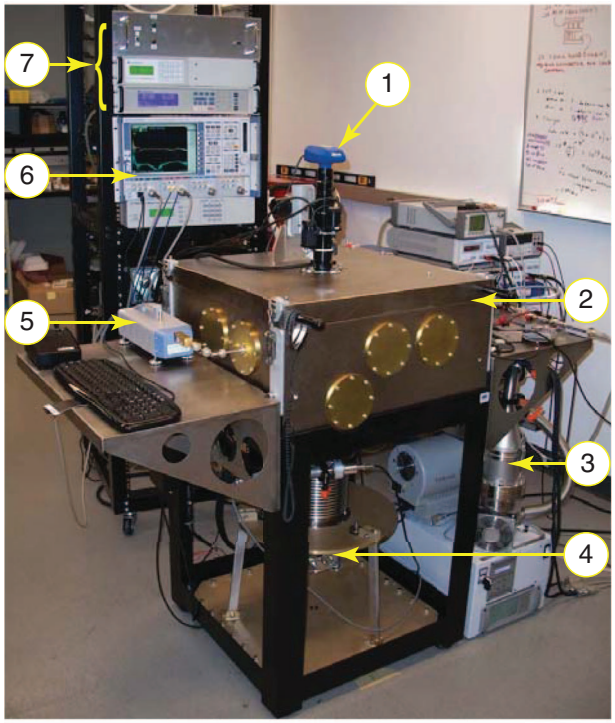

FIG. 1. Completed cryogenic probe station, located in the Cahill Center for Astronomy and Astrophysics at The California Institute of Technology. (1) Microscope and camera, (2) Cryostat, (3) Vacuum pump, (4) Cryocooler, (5) Millimeter wave head, (6) Vector network analyzer (VNA), and (7) Stepper motor, heater, and temperature sensor electronics.

as all moving parts are located inside the cryostat, are maintained at room temperature, and are electrically actuated. This greatly simplifies the mechanical design and packaging of the system.

In order to improve the serviceability of the station, as well as allow for rapid reconfiguration, the probe station is comprised of three sub-assemblies, illustrated in Figure 2 and described as follows:

TABLE I. Cryogenic probe station specifications.

Parameter	Specification
Chuck temperature	≤20 K
Cool down time	≤8 h
Sample size	ø100 mm
RF probe range	± 6.35 mm X-Y-Z[a]
Chuck range	± 50 mm X-Y, 6.35 mm Z[b]
RF frequency	DC-116 GHz

[a]Required probe range of motion is ∼1 mm, half the largest physical dimension of the devices to be measured.
[b]Binary motion for step and repeat testing.

Chuck Positioner: Moves the 114 mm chuck over a ±50 mm range in X and Y and pistons the chuck 6.35 mm in Z. It is rigidly mounted to the floor of the cryostat.

Platen: Holds up to 4 probe positioners, each with ±6.35 mm range of motion in X,Y, and Z. It is mounted to the chuck positioner via adjustable standoffs.

Refrigeration: Provides cooling of the chuck and probes through the use of flexible oxygen-free copper (OFC) heat straps. The first stage of its cryocooler shields the second stage cold finger assembly and also cools the radiation shield surrounding the chuck. It requires partial disassembly for integration with the other sub-assemblies.

The Subsections II A-II G detail the design of the sub-assemblies and components comprising the probe station. Equations are provided that give quick physical insight into design trade-offs and limitations. Calculations made using these equations rely on the use of temperature-dependent values of thermal conductivity, heat capacity, and thermal expansion from NIST's cryogenic materials database.[3] The dependence of thermal conductivity on temperature is illustrated in Figure 3 for oxygen-free high thermal conductivity copper (OFHC), G-10 glass reinforced epoxy (G-10) and grade 304

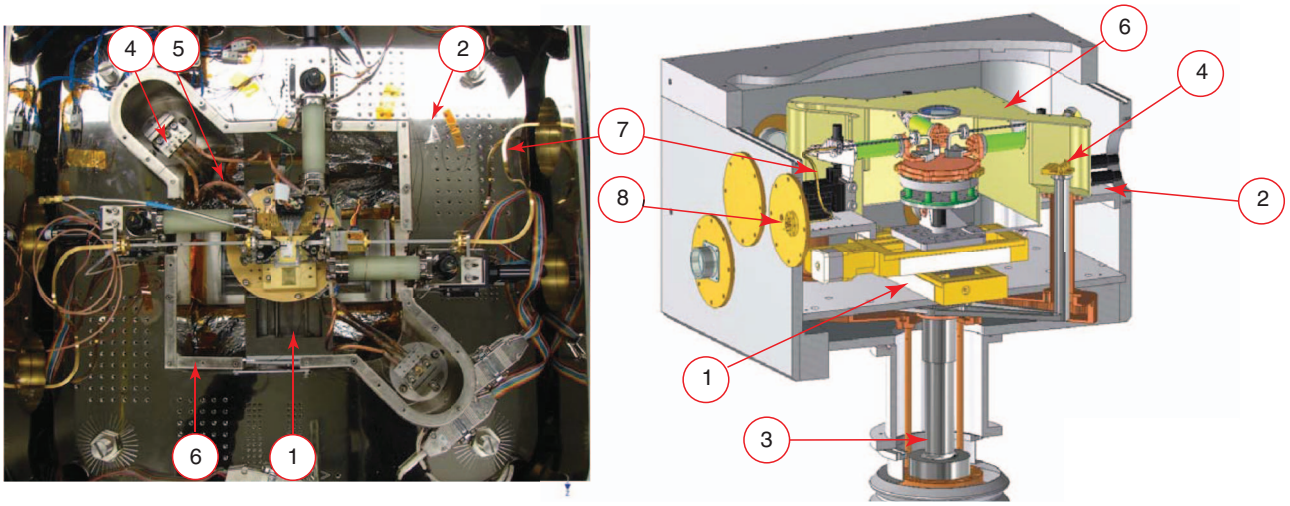

FIG. 2. (Left) Top down photograph of the inside of the cryostat. (Right) Cut-away illustration of the probe station sub-assemblies and components. (1) Chuck positioner sub-assembly, (2) Platen sub-assembly, (3) Refrigeration sub-assembly. Also shown are (4) cold finger heat strap brackets and (5) straps, (6) chuck radiation shield, (7) WR-10 service loop, and (8) WR-10 vacuum feedthrough used to configure the station for measurements at W-band. Chamber external dimensions are 609.6 mm × 609.6 mm × 355.6 mm.

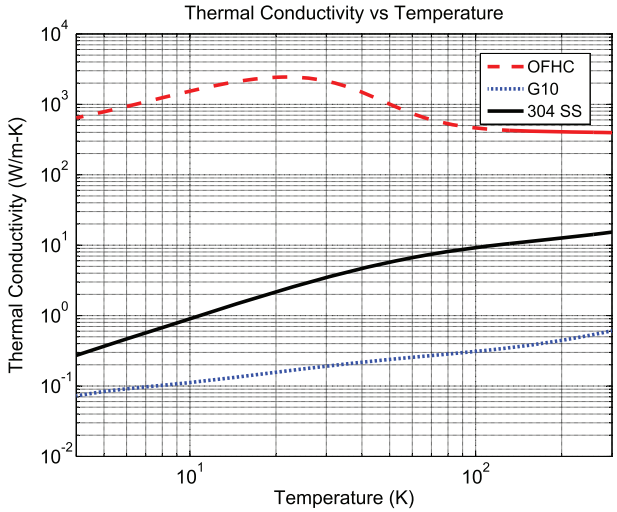

FIG. 3. Thermal conductivities[3] of OFHC, G-10, and 304 stainless steel as a function of temperature. The effect of the conductivity peak in OFHC can be seen in the temperature data presented in Figure 9, where there is a sudden drop in temperatures at ≈3.5 h from the start of the cool down.

stainless steels, all of which are materials employed in the construction of the probe station.

A. Chuck positioner sub-assembly

The chuck positioner is shown in Figure 4. Two 100 mm, vacuum compatible, translation stages (p/n UTSPPV6 from Newport[4]) are used to provide X-Y motion for the chuck assembly, shown on the right of the same figure. It utilizes a G-10 spacer and radiation shield to isolate the chuck base (room temperature) from the chuck above (cooled to <20 K). The conducted heat load from the G-10 spacer was calculated using the temperature-dependent thermal conductivity of G-10, shown in Figure 3, and the relation

$$P_{cond} = \frac{A_{norm}}{l}\int_{T_1}^{T_2} k(T)\,dT, \tag{1}$$

where, A_{norm} is the area of the G-10 isolator normal to conducted heat flow (84 mm^2) and l is the length (28 mm), resulting in a conducted heat load of 332 mW.

The radiated power between two surfaces, with areas A_2 and A_1, may be calculated using[5]

$$P_{rad} = \epsilon_{12}F_{12}A_1\left(T_2^4 - T_1^4\right), \tag{2}$$

where, the effective emissivity, ϵ_{12}, and configuration factor, F_{12}, depend on the materials and geometry of these two surfaces. For large parallel plates, $F_{12} = 1$ and ϵ_{12} is given by

$$\epsilon_{12} = \frac{A_2\epsilon_1\epsilon_2}{A_2\epsilon_2 + A_1\epsilon_1\left(1-\epsilon_2\right)}. \tag{3}$$

Equations (2) and (3) may be used to estimate the radiated heat load from the top of the heat shield to the bottom of the chuck, given that both are polished, gold plated surfaces ($\epsilon_1 = \epsilon_2 = .03$).[6] The resulting heat load is 72 mW. Additional relations for ϵ_{12} and F_{12}, for different geometries, can be found in introductory texts on heat transfer.[6] These relations quickly become complicated and the large parallel plate example is most suited for quick estimates of radiated heat load.

A stepper motor (Lin Engineering[7] p/n 4118S-15-31RO) provides binary motion of 6.35 mm in the z-direction. This is accomplished through the use of a hardened steel cam-lobe mounted to the stepper motor shaft, which rides against a roller-bearing mounted on the bottom of the chuck base. The chuck base translates up and down on a ball-spline bearing assembly prepared for vacuum use (THK (Ref. 8) p/n LF10-3.34LES). One of the benefits of using a stepper motor in this configuration is that it can be stalled without risk of damage to the motor. This allows the use of a cam stop providing repeatable vertical displacement of the chuck. A heater located on the stepper motor mounting plate ensures that the temperature of the stepper motor, ball spline bearing, and translation stages are maintained within their specified operating temperature range.

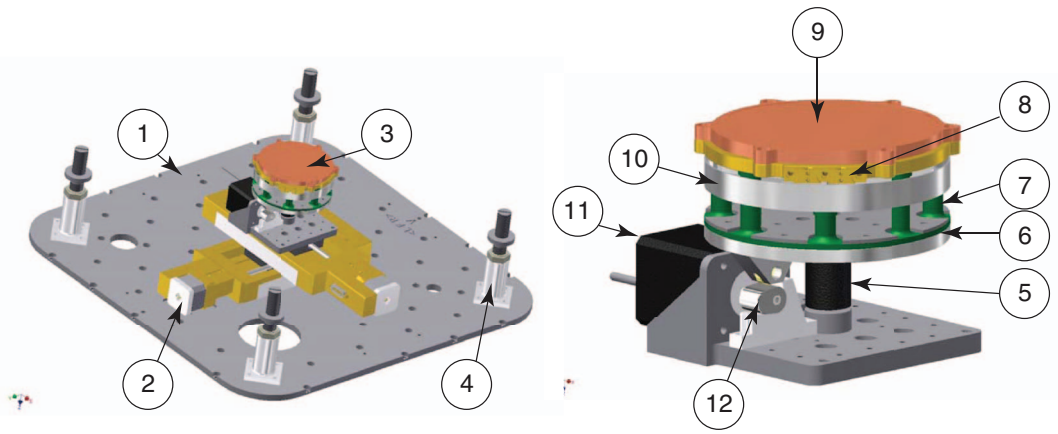

FIG. 4. (Left) Chuck positioner sub-assembly. (1) Mounting plate, (2) 100 mm translation stage, (3) chuck assembly, (4) platen mounts. (Right) Chuck assembly. (5) Ball-spline bearing, (6) chuck base, (7) G-10 isolator, (8) chuck (thermally connected to cold fingers with 8 gauge OFC cable, not shown), (9) wafer holder, (10) radiation shield, (11) stepper motor, and (12) cam lobe.

B. Platen sub-assembly

The platen assembly, shown in Figure 5 holds up to 4 probe positioners (Quater[9] p/n XYZ500MIMT), bolted to a 10 mm aluminum plate. This plate is mounted to the bottom plate of the chuck positioning assembly through 4 adjustable standoffs which afford planarity adjustment. Thermal isolation between the probe and the probe holder is accomplished with tubes machined from G-10 rod. For the W-band measurements presented in Sect. III, a 127 mm length of WR-10 stainless steel waveguide (wall thickness 0.254 mm) is connected between the probe positioner (warm) and probe (cold). The length of the waveguide was optimized for its thermal load and equalization of its thermal expansion, compared to that of the G-10 probe arm. Each probe arm and waveguide yields a conducted heat load of 280 mW and 52 mW, respectively. Although methods exist to plate WR-10 waveguide with one to two skin depths of gold,[10,11] thereby lowering the electrical loss, this increases the thermal load. Fortunately, the vector network analyzer (VNA), described in part E, has adequate power at W-band so that the electrical loss of the unplated waveguide could be accommodated.

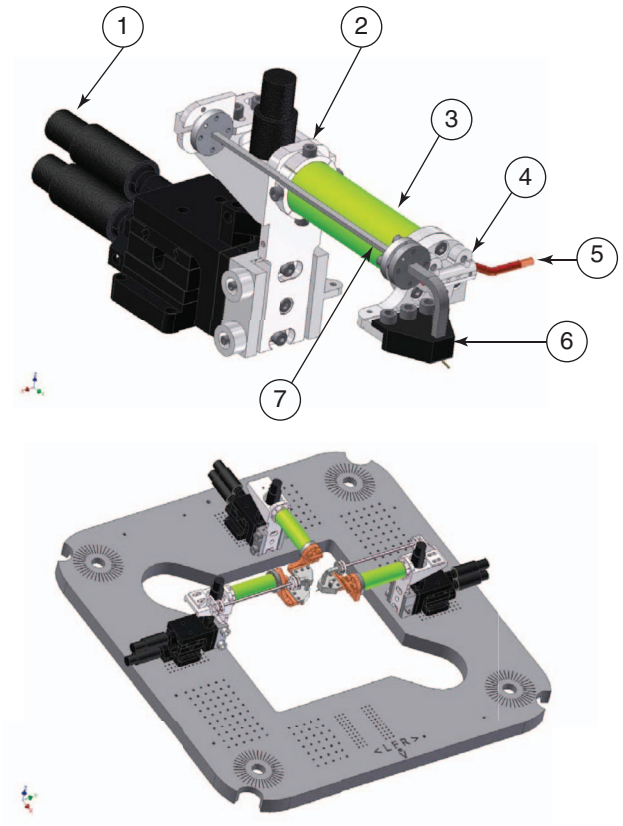

FIG. 5. Probe Positioner Assembly (Top). (1) Quater XYZ500MIMT positioner (2) Probe arm holder. (3) G-10 probe arm (4) Probe holder, connected to the cold fingers with 8 gauge OFC cable (5), (6) WR-10 to CPW probe, (7) WR-10 stainless steel waveguide. Items (6) and (7) may be replaced with different combinations of waveguide/coaxial line and probe for measurements over different frequency ranges. Platen Assembly (Bottom), is comprised of up to 4 probe positioner assemblies (3 shown), mounted to a 10 mm thick aluminum plate.

C. Refrigeration

The design of the refrigeration sub-system is centered around Sumitomo's[12] RDK-415D, Gifford McMahon (GM) cryocooler, capable of 4.2 K at 1.5 W. The sub-assembly is shown in Figure 6. The top of the cryocooler attaches to the bottom of the cryostat through a bellows which provides mechanical isolation. The bottom of the cryocooler is supported by the probe station's steel frame through rubber mounts, to help dampen the cryocooler's vibration. The cooler's second stage is shielded by its first stage via a manifold system, which is also used to mount the radiation shield that encloses the entire chuck assembly. All cold finger assemblies were machined from OFHC, polished, and plated with electroless nickel (emissivity $\approx$0.1). The emissivity of electroless nickel is three times that of gold, but is much less expensive and offers excellent corrosion resistance.[13]

The design of the cold fingers was optimized for thermal resistance versus cool-down time. Increasing the cross-sectional area of the cold fingers lowers the temperature differential across them, but increases their cooling time due to the increased heat capacity. To estimate the cool-down time, data from NIST's cryogenic materials database[3] was again used as the specific heat of most materials is a strong function of temperature. The cool-down time may be estimated using

$$t_{cool} = m \int_{T_1}^{T_2} \frac{c_v(T)}{P_{cool}(T)}\, dT, \tag{4}$$

where, m is the mass of OFHC to be cooled and $c_v(T)$ is its specific heat. $P_{cool}(T)$ is a function of the heat load on the cryocooler, and is therefore a function of component temperature within the cryostat. An analytical expression for $P_{cool}(T)$ was not available and this quantity was instead assumed to be

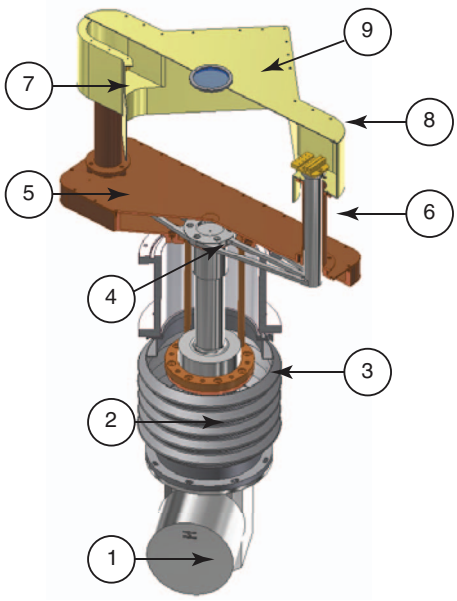

FIG. 6. Cut-away assembly view of refrigeration system. (1) Sumitomo GM Cryocooler, (2) bellows, (3) 1st stage cold finger assembly, (4) 2nd stage cold finger assembly, (5) 1st stage manifold, (6) Attachment point for OFC straps to chuck and probes, (7)(8) Chuck radiation shield, and (9) IR-reflecting window.

constant. Using a value of 15 W at 10 K, from the load map of the Sumitomo cryocooler, the station was estimated to reach <20 K in 4.1 h. The actual cool-down time to 20 K is 3.5 h, as shown in Figure 9.

The use of indium foil and Apiezon-N grease[14,15] was not found to improve thermal resistances of bolted joints within the refrigeration sub-assembly. It is reasoned that this is due to the quality of the machining, polishing, and plating of these components. The only exception was the inclusion of indium foil between the cryocooler's 2nd stage and its cold finger assembly, which was found to make a modest improvement of 0.2 K.

The vibration analysis of the Sumitomo cryocooler was investigated by Tomaru *et al.*,[16] who determined that the two dominant sources of cryocooler vibration are due to its displacer and He pressure oscillations within the cold stages. The cryocooler's vibration is mitigated in part by the use of a bellows and rubber mounts. Also, flexible heat straps from the cold fingers (rigidly mounted to the cryocooler) to the probes and chuck are used to provide thermal conduction and mechanical isolation. These straps are manufactured from 8 gauge OFC speaker wire, soldered to OFHC brackets bolted to the cold fingers, chuck, and probes. Vibration coupling to the chuck and probe arms has not yet been measured, but we estimate the differential displacement to be ~4 μm (the approximate resolution of our optical system) as movement of the probes relative to chuck is barely visible under high magnification.

D. Chamber and vacuum system design

The cryostat's chamber was machined out of M-1 aluminum "mold" plate from Alpase.[17] The mechanical properties of M-1 are similar to that of 6061-T6 aluminum (Young's modulus = 74 GPa for M1 plate and 69 GPa for 6061-T6), but M-1 has a lower cost and is more readily available in large sizes. The chamber could have been fabricated from welded plate, but fabrication costs were estimated to be five times that of the machined version. The chamber interior dimensions measure 572 mm × 572 mm × 238 mm. The chamber walls need to be thick enough to maintain a suitable safety factor between stress on the chamber and the yield strength of the material the chamber is constructed from. Approximate relations for the maximum deflection, δ, and stress, S, for rectangular plates are given by[18,19]

$$\delta = \kappa \frac{L^4 \Delta P}{E t^3}, \tag{5}$$

$$S = \beta \frac{L^2 \Delta P}{t^2}, \tag{6}$$

where, κ and β are dimensionless factors depending on the aspect ratio of the plate and how its edges are supported ($\kappa = 0.0443$ and $\beta = 0.28$ for simply supported square plates), L is the rectangle's shorter dimension, ΔP is the pressure differential, E is Young's modulus, and t is the thickness. The largest calculated deflection is 3.4 mm occurring in the cryostat's lid (machined from 12.7 mm thick 6061-T6 plate instead of M-1 aluminum plate). The corresponding stress is 58 MPa, yielding a safety factor of >4 when compared to the yield strength. The measured deflection of the lid under high vacuum was ≈2 mm, indicating that the above relations were slightly conservative. The majority of the chamber's floor is 51 mm thick, to minimize deflection which would potentially bind the 100 mm translation stages of the chuck positioner sub-assembly. The interior of the chamber was polished and plated with electroless nickel, reducing the radiation load to the cold components and offering a surface that is easily cleaned.

The vacuum system was developed to meet three design criteria: (i) the chamber should reach 1 mTorr within 15 min. (this pressure level is recommended as a startup condition for the cryocooler); (ii) the residual pressure inside the chamber should be lower than 10 μTorr; and (iii) the selected pump(s) should be dry to prevent back-streaming of oil to the chamber and contamination of the samples. The vacuum system was designed according to guidelines and nomograms in.[20]

The vacuum system was provided by Varian, Inc. (now Agilent Technologies[21]) and consists of a turbo-molecular pump (Turbo-V 301 Navigator) connected to the chamber via a manual valve and a 1 m-long hose with KF-40 connectors. The turbo-pump is followed by a backing pump (SH-110) that assists the pump-down at high pressure (viscous regime) inside the chamber. There are two pressure gauges attached to the chamber, a ConvecTorr gauge that covers 760–10^{-4} Torr and an Inverted Magnetron gauge (IMG-100) to cover 10^{-3}–10^{-9} Torr. Pumps and gauges are connected to a controller (XGS-600) which is managed by a computer via a serial connection. This system can reach the 1 mTorr level needed to start the cryocooler in 8 min. At full turbo-rotational speed, the pump-down rate is ~17 l/s and the residual pressure when cryocooling is ~170 nTorr.

E. RF

The probe station has the ability to measure both S-parameters and noise temperature of MMIC amplifiers. The current configuration covers a frequency range of 75–116 GHz and requires internal reconfiguration of the RF components to enable both sets of measurements. As a result, two cool downs are currently needed to perform both S-parameter and noise temperature measurements. In this section, we describe the design of the measurement system used to characterize W-band MMIC amplifiers with the cryogenic probe station.

1. W-band S-parameter setup

For S-parameter measurement, a VNA (Rohde & Schwarz[22] (R&S) ZVA-24, 4 ports) with frequency coverage up to 24 GHz is used. Frequency conversion to W-band is accomplished with millimeter-wave extender heads (R&S ZVA-Z110) custom-tuned to cover 75–116 GHz and with a custom variable attenuation range of around 60 dB to prevent saturation of high gain MMIC amplifiers.

The RF interfaces between the VNA and the cryostat are WR-10 waveguide feedthroughs (Aerowave[23] P/N

10-1662), a simplified version of the WR-10 feedthroughs designed for the ALMA project.[24] The vacuum seals in the WR-10 feedthroughs are pieces of commercial low density polyethylene, which exhibits low microwave loss at the frequencies of interest but has low tensile strength compared to Mylar. This means the windows need to be replaced relatively often (around every 5 months). On the internal side of the chamber, the WR-10 feedthrough connects with a waveguide service loop, the other end of which is mechanically attached to the probe positioner assembly (see Figure 2 and 5). The waveguide service loop was designed to provide enough flexibility to accommodate the (limited) movement of the probe positioners. This part was fabricated from a single piece of thinned-wall coin silver waveguide, then gold plated, by Custom Microwave Inc.;[25] the average insertion loss was ∼0.4 dB across W-band. The thermal break between the room-temperature service loop and the cryogenic wafer probes is provided by a stainless steel (SS) WR-10 waveguide section, with an insertion loss of ∼2.5 dB. Finally, the WR-10 microwave cryogenic probes (GGB (Ref. 26) Picoprobe Model 120) couple the electrical signal at the SS waveguide output to the co-planar waveguide (CPW) probe tips through a waveguide/CPW transition. The W-band insertion loss per probe is 0.75–1.5 dB. The bias to the MMIC samples is provided with dc bias probes (GGB Multi-Contact Wedges) which include bypass capacitors selected for cryogenic operation to mitigate potential high frequency oscillations from the MMIC amplifiers. VNA calibration, at both room temperature and cryogenic conditions, is achieved by landing the probes on CPW calibration standards (GGB CS-5 calkit), mounted to the chuck. The calibration method is thru-reflect-load (TRL). A schematic of the S-parameter setup for the probe station is shown in the top of Figure 7.

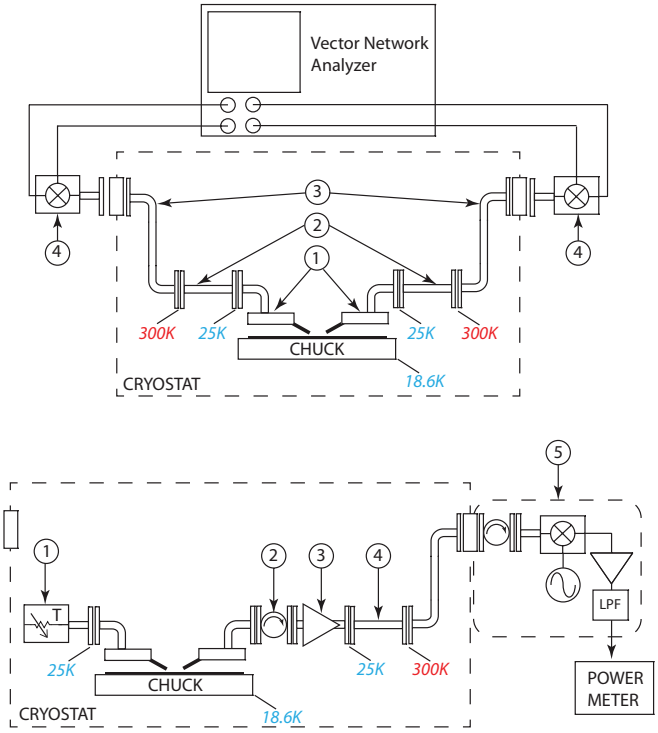

FIG. 7. (Top) S-parameter test setup. (1) WR-10 probes, (2) Stainless steel WR-10 waveguides, (3) WR-10 service loop, and (4) millimeter wave heads. (Bottom) Noise temperature test setup. (1) Variable temperature load, (2) cooled isolator, (3) cooled pre-amplifier, (4) Stainless steel WR-10 waveguide, and (5) Down conversion block. Physical temperatures are indicated to help illustrate thermal paths within the measurement chain. Nominal probe temperature is 25 K, and changes slightly based on the configuration (S-parameter or noise measurement) of the system.

2. Noise temperature measurement setup

The bottom of Figure 7 shows the configuration of the probe station for noise temperature measurements. The SS section connected to the waveguide flange of the input probe is replaced with a variable-temperature load (VTL). The VTL consists of a WR-10 50 Ω termination with a heater and thermometer attached to the waveguide flange. At the RF output, the SS section is reduced in length and the output probe is now followed by a cooled W-band isolator and a packaged W-band LNA, serving as a cooled RF backend amplifier. The isolator is used to improve the impedance match between the device under test (DUT) and the cooled LNA that follows. The packaged LNA is included to allow noise/gain characterization at frequencies where the gain of the DUT is low, and is cryogenically cooled to minimize its contribution to the total receiver noise. Outside the cryostat, an isolator followed by a double-sideband heterodyne receiver connect to the output WR-10 feedthrough. The mixer used in the receiver is a WR10.0SHM sub-harmonic mixer from Virginia Diodes, Inc.[27] and is coupled to the waveguide feedthrough of the cryostat with a waveguide isolator. The local oscillator signal for the mixer is swept to cover the full RF band. The intermediate frequency (IF) chain of the receiver is a combination of baseband amplifiers and low pass filters from Mini-Circuits[28] providing the receiver with a resolution bandwidth of 1 GHz. The IF power is detected with a commercial power sensor and power meter (Agilent's E4412A and E4416A, respectively).

The noise temperature of the DUT is determined using the Y-factor method,[29] as follows. Both RF probes are landed on the DUT and the physical temperature of the VTL is varied between two states ($T^H_{load,Rx}$ and $T^{\mathrm{C}}_{load,Rx}$). The IF output power is recorded at each temperature (P^H_{Rx} and P^C_{Rx}). The DUT is then replaced with a CPW through-line for backend noise characterization and the previous measurement repeated, obtaining two power readings (P^H_{BE} and P^C_{BE}) for the two temperatures of the VTL ($T^H_{load,BE}$, $T^C_{load,BE}$). The noise temperature of the LNA is then found by correcting the measured receiver noise temperature for the noise contribution of the backend (i.e., the components following the LNA in the receiver chain), using the Friis formula,[30]

$$T_{Rx} = T_{DUT} + \frac{T_{BE}}{G_{DUT}}, \tag{7}$$

where, T_{Rx} is the receiver noise temperature, T_{DUT} and T_{BE} are the noise temperatures of the DUT and backend, respectively, and G_{DUT} is the gain of the DUT derived from the power measurements as follows:

$$G_{DUT} = \frac{P_{Rx\,H} - P^C_{Rx}}{P^H_{BE} - P^C_{BE}} \cdot \frac{T^H_{load,BE} - T^C_{load,BE}}{T^H_{load,Rx} - T^C_{load,Rx}}. \tag{8}$$

In the above calculations, the effective load temperatures for the DUT and backend measurements are corrected for the insertion loss of the waveguide probes.

F. Control system and monitoring

The computer interface for the probe and chuck positioners is written in LabView.[31] Communication between the computer and the positioners takes place via general purpose interface bus and serial interfaces. The monitoring readout includes the internal cryostat pressure, 12 temperature sensors inside the cryostat, as well as bias values for the DUT and cold RF amplifier. The control signals include set-point values for the positioners (which are operated open loop) and for a number of PID temperature-control loops.

G. Optical system

The optical system for the probe station consists of a microscope with a digital camera externally mounted to the cryostat, a vacuum window on the cryostat lid and an infrared-blocking window on the chuck radiation shield.

The requirement for this system was to achieve resolution of a few microns at a working distance of around 109 mm (the distance from the top of the raised chuck to the exterior of the vacuum window). The microscope should be able to achieve a zoom range of $\sim$10 $\times$. This is needed since typical operation requires high magnification to land on calibration standards and MMICs as well as lower magnification to navigate from chip-to-chip on a wafer. The zoom adjustment should be motorized to allow fine control and facilitate automation. The field-of-view at low magnification should be sufficient to image a number of MMIC chips at once.

We selected the Navitar[32] 12 $\times$ Zoom system with a 0.75 $\times$ objective lens (which gives a working distance of 108 mm) and the PAXcam5 (Ref. 33) digital microscope camera. With a 1.33 $\times$ adapter and the camera's 1/2 in. CMOS sensor format, the specified field-of-view is in the range 1.1–13.8 mm and the nominal zoom range is 0.87–10.5. At high magnification, this system has a specified resolution of 4 μm. We believe the actual resolution is close to this value, based on the optical quality of the vacuum and shield windows, used in the station's lid and radiation shield, respectively. Based on tests performed using a ring and co-axial light, a ring light was found to give the best performance for the sample materials and optical configuration under consideration. A light emitting diode (LED)-based light source (Dolan-Jenning p/n LMI-6000) was selected to minimize heating of the device under test.

In addition to its ability to withstand vacuum, the vacuum window was selected to have high optical transmission. A synthetic quartz window of diameter 70 mm (VACOM (Ref. 34) p/n ISOVPZ63QTCRSV) was chosen. This window material has low reflection loss (3.5%) and high transmission (93.13%). Due to time constraints, the window was not anti-reflection coated, but this does not appear to have been necessary. For the shield window, a "hot mirror" (Tiffen p/n 55SHM) was used to minimize transmission of infrared wavelengths to the cold wafer probes and the DUT.

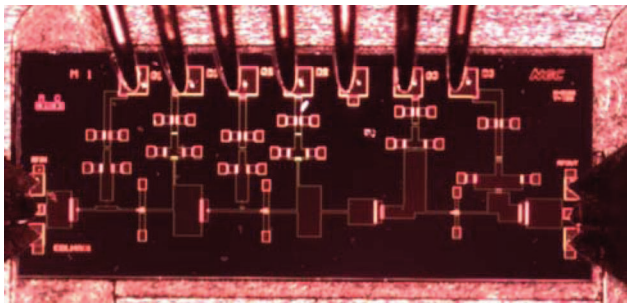

FIG. 8. This image was taken using the PAXcam5 digital camera mounted on the Navitar 12 $\times$ Zoom microscope and shows the W-band wafer probes landed on the input (left) and output (right) of a EBLNA81 amplifier,[2] which is 2.1 mm $\times$ 0.82 mm. Also shown is the DC bias probe landed on the seven bias pads at the top of the image.

Figure 8 shows an example of an image taken using the optical system described above.

III. PERFORMANCE

Temperatures at various locations within the cryostat versus cool-down time are shown in Figure 9, where it can be seen that the chuck temperature reaches <20 K in under 4 h. From the final chuck temperature of 18.6 K and the load map of the Sumitomo cryocooler, it is estimated the total heat load on the cooler is $\approx$6 W. Of this, 1.3 W is due to conduction and radiation from the chuck's heat shield, as summarized in Table II. The remaining 4.7 W radiative heat load is due to coupling between the cryostat floor (warm) and chuck (20 K) part of which is reflected from the radiation shield surrounding the chuck. Although the chuck reaches <20 K in under 4 h, it takes 8 h to stabilize to within $\pm$0.1 K, as preferred for noise measurements. This is probably due to radiative coupling between the chuck and its radiation shield, as the shield

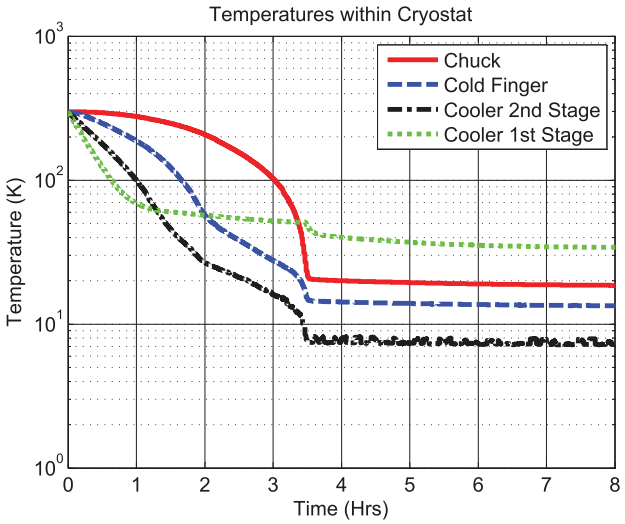

FIG. 9. Temperatures within cryostat versus time. The chuck reaches <20 K in under 4 h. Final temperatures are 18.6 K for the chuck, 13.5 K for the 2nd stage cold finger assembly, 6.8 K at the 2nd stage of the cryocooler, and 34 K at the 1st stage of the cryocooler, reached after 8 h. From the final stage temperatures, we estimate the load on the cryocooler's second stage to be $\approx$6 W.

TABLE II. Heat loads presented to cryocooler.

Path	Material/Finish	Heat Load
Probe arms[a]	G10	(3) × 280 mW
Waveguides[a]	Stainless steel	(2) × 52 mW
Chuck isolator[a]	G10	332 mW
Heat shield[b]	Polished, Au plated	74 mW
Chamber[b,c]	Polished, Ni plated	4700 mW

[a]Conducted.
[b]Radiated.
[c]Estimated from temperature data from completed station. Includes radiation shield surrounding chuck.

is made out of thin aluminum and takes longer to cool down than the OFHC components of the refrigeration system.

The cryogenic RF performance of the probe station at W-band was evaluated by measuring both S-parameters and noise temperature of 4 MMIC HEMT amplifiers silver epoxied on a piece of 254 μm thick alumina substrate. The substrate was clamped to the cold chuck; a layer of indium was added in the interface between substrate and chuck to improve the thermal conductivity. The MMIC chips selected for the evaluation were "105LN1PQ" designs, a modified version of a 4-stage LNA previously reported,[1] fabricated using the well-established 100 nm gate-length InP HEMT process at Northrop Grumman Aerospace Systems.

A GGB CS-5 calibration substrate was mounted to the chuck with the same method used for the MMICs. The physical temperature of the samples was ∼19 K. In S-parameter mode, the VNA was calibrated using the TRL method, landing the probes on the CS-5 calibration substrate. The post-calibration stability was measured by landing one of the probes on a CS-5 short standard at time intervals of approximately 1 h over a 7-h period. The probe was exercised as usual between measurements. The stability results presented in Figure 10 show a full-band average calibration drift of 0.04 dB in 7 h. This suggests that re-calibration of the VNA

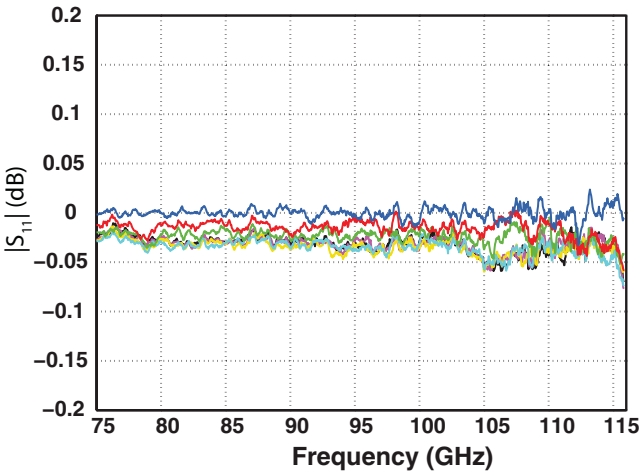

FIG. 10. VNA cryogenic post-calibration stability. A probe was landed on CS-5 short standard and exercised between measurements. Each trace corresponds to a measurement taken at 1 h intervals, drifting from 0 dB to 0.04 dB average in 7 h. This corresponds to a calibration error of ≈−45 dB, which is at least an order of magnitude better than required for our testing purposes.

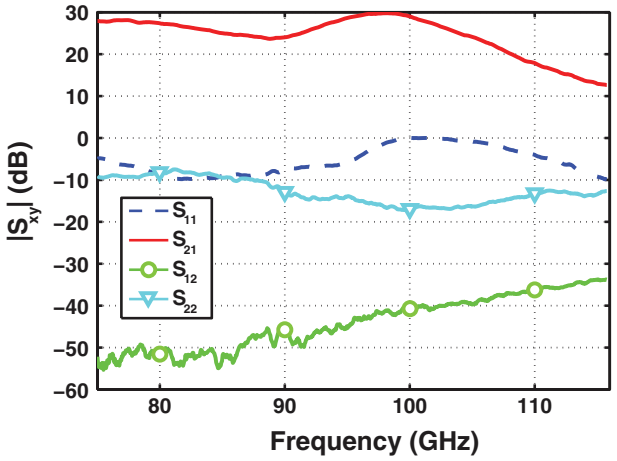

FIG. 11. Cryogenic S-parameters of a 4-stage 105LN1PQ MMIC LNA.[1] Bias conditions are $V_g = 200$ mV, $V_d = 750$ mV, and $I_d = 10$ mA.

is not needed over such a period. Figure 11 shows the full 2-port S-parameters of one of the amplifiers in the sample. The drain voltage (V_d), gate voltage (V_g), and drain current (I_d) for the measurement were $V_d = 750$ mV, $V_g = 200$ mV, and $I_d = 10$ mA, respectively. If the electrical and thermal conditions for the MMIC chips are replicated in a subsequent cool down, then the RF results can be repeated with high precision.

Once the cryogenic S-parameter measurements of all 4 chips were taken, the cryogenic probe station was warmed up and re-configured for noise measurements. Following the methodology presented earlier, DUT cryogenic noise temperatures and gains were derived from Y-factor measurements. The physical temperature of the VTL was varied from 30 K to 55 K, while the physical temperature for the samples varied by ∼0.5 K during the exercise. A noise/gain plot with results from the measurements is shown in Figure 12. The results from both measurement setups can be cross-checked by comparing S_{21} (VNA measurement) and the DUT derived gain from the noise measurement. The requirement, again, is that the electrical and thermal conditions for the MMICs are repeated between measurements. Such comparison is presented

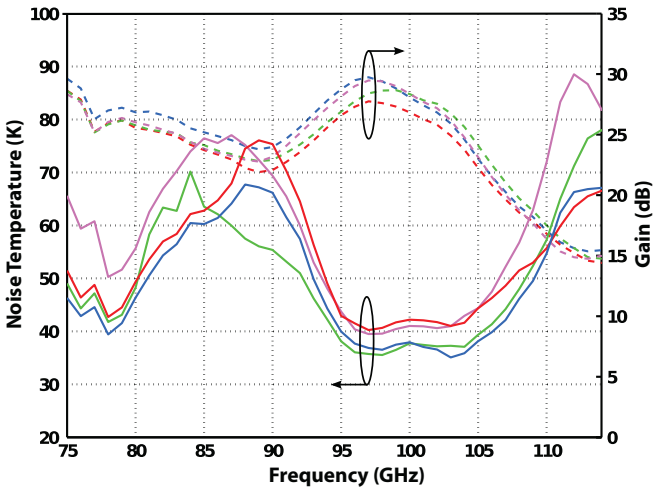

FIG. 12. Cryogenic noise/gain characteristic of the four 105LN1PQ MMIC LNAs. Each color trace corresponds to an individual MMIC chip.

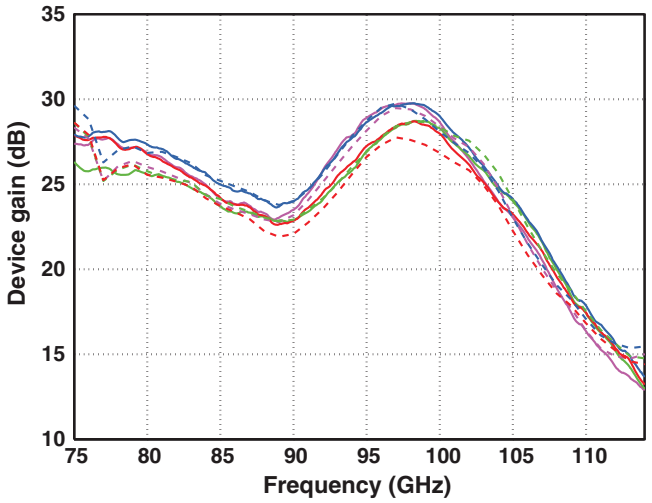

FIG. 13. Comparison between derived gain from Y-factor based noise measurements (dashed lines) and S_{21} from independent S-parameter measurements (solid lines). Each color trace corresponds to a single 105LN1PQ MMIC chip.

in Figure 13 and shows excellent agreement between the two setups.

IV. FUTURE IMPROVEMENTS

The cryogenic probe station is currently being utilized to screen W-band MMIC LNAs for several projects within radio-astronomy. The station will be updated in the near future for DC-67 GHz measurements, replacing the WR-10 waveguide and feedthroughs with stainless steel UT-47 coaxial cable from Micro-Coax[35] and V100 hermetic glass beads from Anritsu.[36] No degradation of the temperature performance is expected, as it is currently limited by radiative coupling between the cryostat's floor (warm) and chuck (cold).

The authors estimate that any future improvements to the minimum chuck temperature will be limited to a decrease of ≈4 K. Increasing the cross section of the cold fingers connected to the cryocooler's second stage will reduce the chuck temperature at the cost of increased cool-down time. Altering the chuck radiation-shield's (item 7 in Figure 6) material and finish may have the largest impact, as it is suspected that the majority of the radiative load incident on the chuck is reflected off the radiation shield. In the future, the radiation shield will be replaced with one manufactured from OHFC. Although this is not expected to significantly reduce the radiated load, it should help reduce the chuck stabilization time by several hours.

Although we have demonstrated highly repeatable noise temperature measurements, there is a systematic offset of up to 20 K between the noise temperature of W-band amplifiers as measured on the cryogenic probe station and the same amplifier chips when individually packaged. We are therefore working to establish the absolute calibration of the W-band cryogenic probe station noise measurements.

To improve the efficiency of cryogenic noise temperature measurements, we will upgrade the W-band noise measurement to use the "cold attenuator" method[37] instead of the present VTL. This method uses an active noise source, which can be conveniently located outside the cryostat. The RF power emitted by the noise source is coupled to the input wafer probe via a cryogenically cooled ∼20–30 dB attenuator. The cold attenuator prevents the DUT from becoming saturated and improves the matching between the noise source and the DUT. The active noise source can be rapidly switched on/off, enabling a Y-factor measurement between the two states of the noise source. This method change will significantly reduce the measurement time per chip, which is important for screening the large number of devices needed for future focal plane arrays.

V. CONCLUSION

The design and performance of a cryogenic probe station, suitable for electrical characterization of devices from dc–millimeter wave has been presented. The unique design uses electrically actuated positioners, maintained at room temperature, for movement of both the probe positioners and chuck. This greatly simplifies the design and allows for step and repeat testing of wafers up to 100 mm in diameter, at physical temperatures <20 K. Flexible OFC heat straps are used to isolate the cooled chuck and probes from its GM cryocooler, yielding a platform stable enough for highly repeatable measurements at millimeter-wave frequencies. The station's high-frequency probing capability was illustrated with cryogenic S-parameter and noise temperature data for a W-band MMIC LNA currently used within radio-astronomy.

ACKNOWLEDGMENTS

The authors are grateful to the Keck Institute for Space Studies for funding the development of the cryogenic probe station. The authors are very grateful to Mike Martin-Vegue, of MVI Engineering,[38] for the machining, manufacturing, and design support of the probe stations components. The authors also wish to thank Todd Gaier (Jet Propulsion Laboratory) and Glenn Jones, Oliver King, and Sander Weinreb (California Institute of Technology) for helpful discussions and suggestions during the design and manufacturing of the probe station.

[1]W. Weinreb, R. Lai, N. Erickson, T. Gaier, and J. Wielgus, *1999 IEEE MTT-S International Microwave Symposium Digest* (IEEE, Piscataway, NJ, 1999), pp. 101–104.
[2]E. Bryerton, X. Mei, Y. Kim, W. Deal, W. Yoshida, M. Lange, J. Uyeda, M. Morgan, and R. Lai, *2009 IEEE MTT-S International Microwave Symposium Digest* (IEEE, Piscataway, NJ, 2009), pp. 681–684.
[3]E. Marquardt, J. Le, and R. Radebaugh, in *Proceedings of the 11th International Cryocooler Conference* (Keystone, CO, 2000), pp. 1–7.
[4]Newport Corporation, 1791 Deere Ave, Irvine, CA 92606, USA.
[5]R. Barron, *Cryogenic Systems*, 2nd ed. (Oxford University Press, New York, 1985), pp. 386–391.
[6]F. Incropera, D. Dewitt, T. Bergman, and A. Lavine, *Introduction to Heat Transfer*, 5th ed. (Wiley, New Jersey, 2007), pp. 772–793 and p. 863.
[7]Lin Engineering, 16245 Vineyard Blvd., Morgan Hill, CA 95037, USA.
[8]THK America, 200 E. Commerce Dr., Schaumburg, IL 60173, USA.
[9]Quater Research and Development, PO Box 8824, Bend, OR 97708, USA.
[10]G. Petencin, Technical Report (National Radio Astronomy Observatory, Charlottesville, VA, 2005).
[11]B. Shank, J. Heilman, and A. Dahm, Microwave J. **50**, 107 (2007).

[12]Sumitomo Cryogenics of America, 456 Oakmead Parkway, Sunnyvale, CA 94085, USA.
[13]If left unplated, these surfaces would eventually oxidize, causing the emissivity, and therefore heat load on the cooler, to change with time.
[14]A. Kerr and N. Horner, Technical Report No. 163 (National Radio Astronomy Observatory, Charlottesville, VA, 1991).
[15]A. Kerr and R. Groves, Technical Report No. 204 (National Radio Astronomy Observatory, Charlottesville, VA, 2006).
[16]T. Tomaru, T. Suzuki, T. Haruyama, T. Shintomi, A. Yamamoto, T. Koyama, and R. Li, Cryogenics **44**(5), 309 (2004).
[17]Alpase, 9750 Seaaca St, Downey, CA 90241, USA.
[18]W. Nash, *Metals Engineering Design* (McGraw-Hill, New York, 1965), pp. 174–179.
[19]R. Green, *Machinery's Handbook* (Industrial, New York, 1992), pp. 256–258.
[20]A. Roth, *Vacuum Technology* (North-Holland, New York, 1990), pp. 50–148.
[21]Agilent Technologies, 5301 Stevens Creek Blvd., Santa Clara, CA 95051, USA.
[22]Rohde and Schwarz USA, Inc., 8661A Robert Fulton Dr., Columbia, MD 21046-2265, USA.
[23]Aerowave Inc., 344 Salem St., Medford, MA 02155, USA.
[24]G. Ediss, F. Johnson, D. Koller, and A. Kerr, Technical Report No. 536 (National Radio Astronomy Observatory, Charlottesville, VA, 2005).
[25]Custom Microwave Inc., 24 Boston Ct., Longmont, CO 80501, USA.
[26]GGB Industries, PO Box 10958, Naples, FL 34101, USA.
[27]Virginia Diodes Inc, 979 Second Street, Suite 309, Charlottesville, VA 22902-6172, USA.
[28]Mini-Circuits, 13 Neptune Ave., Brooklyn, NY 11235, USA.
[29]D. Pozar, *Microwave Engineering* (Addison-Wesley, Reading, MA, 1990), pp. 588–589.
[30]J. Kraus, *Radio Astronomy* (Cygnus-Quasar Books, Powell, OH, 1986), p. 27.
[31]LabView is a product of National Instruments. National Instruments Corp., 11500 N. Mopac Expwy., Austin, TX 78759, USA.
[32]Navitar Inc., 200 Commerce Drive Rochester, NY 14623, USA.
[33]Paxcam, 707 N. Iowa Ave., Villa Park, IL 60181-1510, USA.
[34]VACOM Vakuum Komponenten & Messtechnik GmbH, Gabelsgergerstraße 9, 07749 Jena, Germany.
[35]Micro-Coax, 206 Jones Blvd., Pottstown, PA 19464, USA.
[36]Anritsu Corporation, 490 Jarvis Dr., Morgan Hill, CA 95037, USA.
[37]G. Fernandez, Technical Report No. 42-135 (Jet Propulsion Laboratory, Pasadena, CA, 1998).
[38]MVI Engineering, 5772 Crown Dr., Mira Loma, CA 91752, USA.